

# Strong charmonium decays in a microscopic model

J. Segovia<sup>a,\*</sup>, D.R. Entem<sup>a</sup>, F. Fernández<sup>a</sup>

<sup>a</sup>*Grupo de Física Nuclear and IUFFyM, Universidad de Salamanca, E-37008 Salamanca, Spain*

---

## Abstract

Although the spectra of heavy quarkonium systems have been successfully explained by certain QCD motivated potential models, their strong decays are still an open problem. We perform a microscopic calculation of vector charmonium strong decays into open-charm mesons where the  $q\bar{q}$  pairs are created from the same interquark interactions acting in the quark model that has been used to describe its spectrum, and also its leptonic and radiative decays. We compare the numerical results with those predicted by the  $^3P_0$  decay model and with the available experimental data, and discuss the possible influence on the strong widths of the different terms of the potential. A comparison with other predictions from similar microscopic decay models is also included.

*Keywords:* Hadronic decay, Heavy quarkonia, Potential models

---

## 1. Introduction

Since its discovery in 1974 [1, 2], the charmonium system has become the prototypical 'hydrogen atom' of meson spectroscopy [3, 4]. The spectrum of relatively narrow states below the open-charm threshold at 3.73 GeV can be identified with the  $1S$ ,  $1P$  and  $2S$   $c\bar{c}$  levels predicted by potential models which incorporate a color Coulomb term at short distances and a color confining term at large distances. Difficulties arises above the open-charm threshold due to the coupling with the meson-meson continuum.

In recent times the construction of  $B$ -factories has triggered the discovery of many new particles, denoted as  $XYZ$  mesons, whose nature supposes a

---

\*Current address: Physics Division, Argonne National Laboratory, Argonne, IL 60439, USA.

challenge for the theorists and can contribute to a better knowledge of the  $c\bar{c}$  phenomenology.

One open topic of great interest on charmonium states is their strong decays which constitute a rather poorly understood area of hadronic physics. A great part of our knowledge of strong interaction comes from decays and for that reason it is important to pursue the most complete description of them.

Attempts of modeling strong decays date from Micu's suggestion [5] that hadron decays proceed through  $q\bar{q}$  pair production with vacuum quantum numbers,  $J^{PC} = 0^{++}$ . Since this corresponds to a  ${}^3P_0$   $q\bar{q}$  state, it is now generally referred to as the  ${}^3P_0$  decay model. This suggestion was developed and applied extensively by Le Yaouanc *et al.* [6, 7] in the 1970s. Studies of hadron decays using the  ${}^3P_0$  model have been concerned almost exclusively with numerical predictions, and have not led to any fundamental modifications to the original model. Recent studies have considered changes in the spatial dependence of the pair production amplitude as a function of quark coordinates [8–11]. There have been some studies of the decay mechanism which consider an alternative phenomenological model in which the  $q\bar{q}$  pair is produced with  ${}^3S_1$  quantum numbers [12]. However, this possibility seems to disagree with experiment [9].

An alternative procedure is the study of strong decays through microscopic decay models. The difference between this approach and those described above lies on the description of the  $q\bar{q}$  pair creation vertex. In the microscopic decay models the  $q\bar{q}$  pair is created from interquark interactions acting in the quark model. The differences between calculations of this kind lies in the choice of the pieces of the potential which enter in the vertex calculation.

So Eichten *et al.* [13, 14] assumes that the  $q\bar{q}$  production is due to the time-like part of the vector Lorentz confining interaction, while Ackleh *et al.* [15] and Bao *et al.* [16] assumes that the  $q\bar{q}$  pair is produced by one-gluon exchange and scalar confining interactions. Then, the description of the strong decays is intimately related with the problem of the Dirac structure of the confinement.

From the point of view of the hadronic spectroscopy, confinement has to be dominantly scalar in order to reproduce the hyperfine splittings observed in heavy quarkonium [17–19], although to explain the light quark phenomenology a small mixture (of the order of 20%) of vector confinement is needed [20]. However, build Hamiltonian-based models of QCD [21] seems

to require vector confinement.

In the present work, we generalize the microscopic decay models of references mentioned above using the quark interaction of Ref. [20] which includes one gluon exchange plus a mixture of scalar and vector confinement. This model successfully describes hadron phenomenology and hadronic reactions and has recently been applied to mesons containing heavy quarks in Refs. [22, 23]. We study the open-charm strong decays of the  $1^{--} c\bar{c}$  resonances looking for the possible influence of the mixture of scalar and vector Lorentz structure.

The content of the present paper is organized as follows. In section 2 we briefly explain the main features of the constituent quark model. Section 3 is devoted to the microscopic description of the strong decay mechanism. Section 4 is dedicated to show our results and how its compared with those of the  $^3P_0$  model. A comparison of the numerical values coming from our microscopic decay model with those of other similar microscopic decay models is also included. We finish in Section 5 with some remarks and conclusions.

## 2. Constituent quark model

One consequence of the spontaneous chiral symmetry breaking is that the nearly massless “current” light quarks acquire a dynamical, momentum-dependent mass  $M(p)$  with  $M(0) \approx 300$  MeV for the  $u$  and  $d$  quarks, namely, the constituent mass. To preserve chiral invariance of the QCD Lagrangian new interaction terms, given by Goldstone-boson exchanges, should appear between constituent quarks. This together with the perturbative one-gluon exchange (OGE) and the nonperturbative confining interactions are the main pieces of our potential model [20].

The wide energy range covered by a consistent description of light, strange and heavy mesons requires an effective scale-dependent strong coupling constant. We use the frozen coupling constant of Ref. [20]

$$\alpha_s(\mu) = \frac{\alpha_0}{\ln\left(\frac{\mu^2 + \mu_0^2}{\Lambda_0^2}\right)}, \quad (1)$$

where  $\mu$  is the reduced mass of the  $q\bar{q}$  pair and  $\alpha_0$ ,  $\mu_0$  and  $\Lambda_0$  are parameters of the model determined by a global fit to all meson spectrum.

In the heavy quark sector chiral symmetry is explicitly broken and Goldstone-boson exchanges do not appear. Only the OGE and confinement potentials

are present and contain central, tensor and spin-orbit contributions. For the OGE potential, they are given by

$$\begin{aligned}
V_{\text{OGE}}^{\text{C}}(\vec{r}_{ij}) &= \frac{1}{4}\alpha_s(\vec{\lambda}_i^c \cdot \vec{\lambda}_j^c) \left[ \frac{1}{r_{ij}} - \frac{1}{6m_i m_j} (\vec{\sigma}_i \cdot \vec{\sigma}_j) \frac{e^{-r_{ij}/r_0(\mu)}}{r_{ij} r_0^2(\mu)} \right], \\
V_{\text{OGE}}^{\text{T}}(\vec{r}_{ij}) &= -\frac{1}{16} \frac{\alpha_s}{m_i m_j} (\vec{\lambda}_i^c \cdot \vec{\lambda}_j^c) \left[ \frac{1}{r_{ij}^3} - \frac{e^{-r_{ij}/r_g(\mu)}}{r_{ij}} \left( \frac{1}{r_{ij}^2} + \frac{1}{3r_g^2(\mu)} + \frac{1}{r_{ij} r_g(\mu)} \right) \right] S_{ij}, \\
V_{\text{OGE}}^{\text{SO}}(\vec{r}_{ij}) &= -\frac{1}{16} \frac{\alpha_s}{m_i^2 m_j^2} (\vec{\lambda}_i^c \cdot \vec{\lambda}_j^c) \left[ \frac{1}{r_{ij}^3} - \frac{e^{-r_{ij}/r_g(\mu)}}{r_{ij}^3} \left( 1 + \frac{r_{ij}}{r_g(\mu)} \right) \right] \times \\
&\quad \times \left[ ((m_i + m_j)^2 + 2m_i m_j) (\vec{S}_+ \cdot \vec{L}) + (m_j^2 - m_i^2) (\vec{S}_- \cdot \vec{L}) \right], \tag{2}
\end{aligned}$$

where  $\vec{S}_{\pm} = \frac{1}{2}(\vec{\sigma}_i \pm \vec{\sigma}_j)$ . Besides,  $r_0(\mu) = \hat{r}_0 \frac{\mu_{nn}}{\mu_{ij}}$  and  $r_g(\mu) = \hat{r}_g \frac{\mu_{nn}}{\mu_{ij}}$  are regulators which depend on  $\mu_{ij}$ , the reduced mass of the interacting quarks. The contact term of the central potential of one-gluon exchange has been regularized in a suitable way as

$$\delta(\vec{r}_{ij}) \sim \frac{1}{4\pi r_0^2} \frac{e^{-r_{ij}/r_0}}{r_{ij}}. \tag{3}$$

The breaking of the color electric string between two static color sources is a phenomenon predicted by QCD and it is the basis of the meson decays and hadronization processes. Although there is no analytical proof, it is a general belief that confinement emerges from the force between the gluon color charges. When two quarks are separated, due to the non-Abelian character of the theory, the gluon fields self-interact forming color strings which bring the quarks together.

In a pure gluon gauge theory the potential energy of the  $q\bar{q}$  pair grows linearly with the quark-antiquark distance. However, in full QCD the presence of sea quarks soften the linear potential, due to the screening of the color charges, and eventually leads to the breaking of the string. We incorporate it in our confinement potential as

$$\begin{aligned}
V_{\text{CON}}^{\text{C}}(\vec{r}_{ij}) &= [-a_c(1 - e^{-\mu_c r_{ij}}) + \Delta] (\vec{\lambda}_i^c \cdot \vec{\lambda}_j^c), \\
V_{\text{CON}}^{\text{SO}}(\vec{r}_{ij}) &= -(\vec{\lambda}_i^c \cdot \vec{\lambda}_j^c) \frac{a_c \mu_c e^{-\mu_c r_{ij}}}{4m_i^2 m_j^2 r_{ij}} \left[ ((m_i^2 + m_j^2)(1 - 2a_s) \right. \\
&\quad \left. + 4m_i m_j(1 - a_s)) (\vec{S}_+ \cdot \vec{L}) + (m_j^2 - m_i^2)(1 - 2a_s) (\vec{S}_- \cdot \vec{L}) \right], \tag{4}
\end{aligned}$$

where  $a_s$  controls the ratio between the scalar and vector Lorentz structure

$$V_{\text{CON}}(\vec{r}_{ij}) = a_s V_{\text{CON}}^{\text{scalar}}(\vec{r}_{ij}) + (1 - a_s) V_{\text{CON}}^{\text{vector}}(\vec{r}_{ij}). \quad (5)$$

At short distances this potential presents a linear behavior with an effective confinement strength  $\sigma = -a_c \mu_c (\vec{\lambda}_i^c \cdot \vec{\lambda}_j^c)$  while it becomes constant at large distances. This type of potential shows a threshold defined by

$$V_{thr} = \{-a_c + \Delta\} (\vec{\lambda}_i^c \cdot \vec{\lambda}_j^c). \quad (6)$$

No  $q\bar{q}$  bound states can be found for energies higher than this threshold and the system suffers a transition from a color string configuration between two static color sources into a pair of static mesons due to the breaking of the color flux-tube and the most favored subsequent decay into hadrons.

To find the quark-antiquark bound states with these interactions, we solve the Schrödinger equation using the Gaussian Expansion Method [24]. It allows us to evaluate easily the strong decay amplitudes.

In this method the radial wave function, solution of the Schrödinger equation, is expanded in terms of basis functions as

$$R_\alpha(r) = \sum_{n=1}^{n_{max}} c_n^\alpha \phi_{nl}^G(r), \quad (7)$$

where  $\alpha$  refers to the channel quantum numbers. The coefficients  $c_n^\alpha$  and the eigenenergy  $E$  are determined from the Rayleigh-Ritz variational principle

$$\sum_{n=1}^{n_{max}} \left[ (T_{n'n}^\alpha - EN_{n'n}^\alpha) c_n^\alpha + \sum_{\alpha'} V_{n'n}^{\alpha\alpha'} c_n^{\alpha'} = 0 \right], \quad (8)$$

where  $T_{n'n}^\alpha$ ,  $N_{n'n}^\alpha$  and  $V_{n'n}^{\alpha\alpha'}$  are the matrix elements of the kinetic energy, the normalization and the potential, respectively.  $T_{n'n}^\alpha$  and  $N_{n'n}^\alpha$  are diagonal whereas the mixing between different channels is given by  $V_{n'n}^{\alpha\alpha'}$ .

Following Ref. [24] we employ Gaussian trial functions whose ranges are in geometric progression. This is useful in optimizing the ranges with a small number of free parameters. Moreover, this distribution of range parameters is dense at small ranges which is well suited for making the wave function correlated with short range potentials. The fast damping of the gaussian tail is not a real problem since we can choose the maximal range much larger than the hadronic size.

Quark mass	$m_c$ (MeV)	1763
Confinement	$a_c$ (MeV)	507.4
	$\mu_c$ (fm <sup>-1</sup> )	0.576
	$\Delta$ (MeV)	184.432
	$a_s$	0.81
OGE	$\alpha_0$	2.118
	$\Lambda_0$ (fm <sup>-1</sup> )	0.113
	$\mu_0$ (MeV)	36.976
	$\hat{r}_0$ (fm)	0.181
	$\hat{r}_g$ (fm)	0.259

Table 1: Quark model parameters.

$J^{PC}$	$n$	$M_{\text{The.}}$	$M_{\text{Exp.}}$	
$1^{--}$	1	3096	$3096.916 \pm 0.011$	[25]
	2	3703	$3686.108^{+0.011}_{-0.014}$	[25]
	3	3796	$3778.1 \pm 1.2$	[25]
	4	4097	$4039 \pm 1$	[25]
	5	4153	$4153 \pm 3$	[25]
	6	4389	$4361 \pm 9 \pm 9$	[26]
	7	4426	$4421 \pm 4$	[25]
	8	4614	$4634^{+8+5}_{-7-8}$	[27]
	9	4641	$4664 \pm 11 \pm 5$	[26]

Table 2: Masses, in MeV, of  $1^{--}$  charmonium states. We compare with the well established states in Ref. [25] and assign possible  $XYZ$  mesons.

Table 1 shows the model parameters fitted over all spectrum of mesons and needed for the heavy quark sector. Note that, once the parameters are fitted, our confinement interaction is dominantly scalar.

Finally, Table 2 shows the masses predicted by our model for the vector charmonium states, the comparison with the experimental data and some possible assignments of  $XYZ$  mesons. Further details on the spectrum and other properties of vector charmonium states can be found in Ref. [22].

### 3. Strong decays

The microscopic decay models are an attempt to describe strong interactions in terms of quark and gluon degrees of freedom. As mentioned above, after the pioneering work of Eichten *et al.* [13, 14] which assume that the strong decays are driven by the time-like component of the confining interaction, only few works have addressed this topic in a partial way without discussing the relationship between this decays and the nature of confinement.

We shall assume that the responsible for the strong decays is the full quark-quark interaction of our model which includes one-gluon exchange, scalar and vector confining interactions, allowing in this way the study of the influence of the different pieces on the final results.

The associated decay amplitudes of the one-gluon exchange and the confinement interactions should be added coherently. Therefore, the current-current interactions can be written in the generic form as [15]

$$H_I = \frac{1}{2} \int d^3x d^3y J^a(\vec{x}) K(|\vec{x} - \vec{y}|) J^a(\vec{y}). \quad (9)$$

The current  $J^a$  in Eq. (9) is assumed to be a color octet. The currents,  $J$ , with the color dependence  $\lambda^a/2$  factored out and the kernels,  $K(r)$ , for the interactions are

- Currents

$$J(\vec{x}) = \bar{\psi}(\vec{x}) \Gamma \psi(\vec{x}) = \begin{cases} \bar{\psi}(\vec{x}) \mathcal{I} \psi(\vec{x}) & \text{Scalar Lorentz current,} \\ \bar{\psi}(\vec{x}) \gamma^0 \psi(\vec{x}) & \text{Time-like vector Lorentz current,} \\ \bar{\psi}(\vec{x}) \vec{\gamma} \psi(\vec{x}) & \text{Space-like vector Lorentz current.} \end{cases} \quad (10)$$

- Kernels

$$K(r) = \begin{cases} -4a_s [-a_c(1 - e^{-\mu_c r}) + \Delta] & \text{Scalar Confinement,} \\ +4(1 - a_s) [-a_c(1 - e^{-\mu_c r}) + \Delta] & \text{Static Vector Confinement,} \\ -4(1 - a_s) [-a_c(1 - e^{-\mu_c r}) + \Delta] & \text{Transverse Vector Confinement,} \\ +\frac{\alpha_s}{r} & \text{Coulomb OGE,} \\ -\frac{\alpha_s}{r} & \text{Transverse OGE.} \end{cases} \quad (11)$$

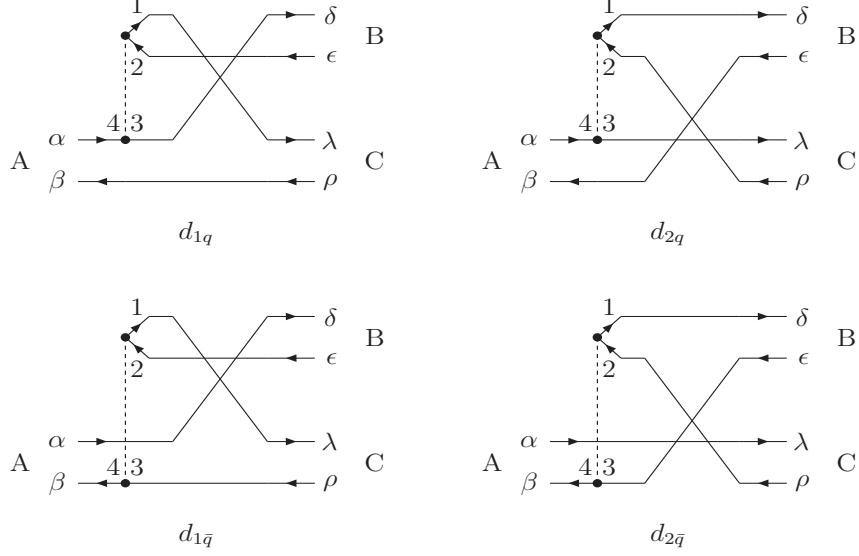


Figure 1: Diagrams that contribute to the decay width through the microscopic model.

Following Ref. [15], we refer to this general type of interaction as a  $JKJ$  and to the specific cases considered here as  $sKs$ ,  $j^0Kj^0$  and  $j^TKj^T$  interactions. Details of the resulting matrix elements for different cases are given in Appendix A.

The diagrams that contribute to the strong decay  $A \rightarrow B + C$  are shown in Fig. 1. There are two coming from the quark line,  $d_{1q}$  and  $d_{2q}$ . The difference between them is the rearrangement of the quarks and antiquarks in the final mesons. The other two diagrams are referred to the antiquark line,  $d_{1\bar{q}}$  and  $d_{2\bar{q}}$ .

The total width is the sum over the partial widths characterized by the total spin,  $J_{BC}$ , and the relative angular momentum,  $l$ , of the final mesons  $B$  and  $C$

$$\Gamma_{A \rightarrow BC} = \sum_{J_{BC}, l} \Gamma_{A \rightarrow BC}(J_{BC}, l), \quad (12)$$

where

$$\Gamma_{A \rightarrow BC}(J_{BC}, l) = 2\pi \int dk_0 \delta(E_A - E_{BC}) |\mathcal{M}_{A \rightarrow BC}(k_0)|^2 \quad (13)$$

and  $\mathcal{M}_{A \rightarrow BC}(k_0)$  is calculated following Appendix A.



Using relativistic phase-space we arrive at

$$\Gamma_{A \rightarrow BC}(J_{BC}, l) = 2\pi \frac{E_B E_C}{m_A k_0} |\mathcal{M}_{A \rightarrow BC}(k_0)|^2, \quad (14)$$

where

$$k_0 = \frac{\sqrt{[m_A^2 - (m_B - m_C)^2][m_A^2 - (m_B + m_C)^2]}}{2m_A} \quad (15)$$

is the on-shell relative momentum of mesons  $B$  and  $C$ .

We will compare our results with the widely used  ${}^3P_0$  decay model which is a particular case of Eq. (11) with only a constant scalar term  $S_0 = \frac{3^{5/2}}{2^4} m_q \gamma$ . A complete development of this model can be found in Ref. [28].

#### 4. Results

From an experimental point of view there are a few data in the open-charm decays of the  $1^{--} c\bar{c}$  resonances. The main experimental data are the resonance parameters, mass and total decay width, of the excited  $\psi$  states.

Tables 3 and 4 show the strong decay widths predicted by the microscopic model for the  $1^{--} c\bar{c}$  states established in Table 2 compared with the experimental data and the  ${}^3P_0$  results. The parameter  $\gamma$  of the  ${}^3P_0$  model has been fitted in Ref. [29]. The notation  $D_1 D_2$  includes the  $D_1 \bar{D}_2$  and  $\bar{D}_1 D_2$  combination of well defined  $CP$  quantum numbers. For the kinematics we use experimental masses whenever they are available.

One can see that the total decay widths predicted by the microscopic model are in general lower than the experimental ones, whereas those predicted by the  ${}^3P_0$  model reproduce the data in a better way. However, it is worth to notice that the correct order of magnitude of the strong decays is given by the microscopic model with no free parameter in contrast with the one parameter of the  ${}^3P_0$  model.

When we go up through the spectrum, the states are more and more wide and the total widths for  $S$  and  $D$ -waves are larger in both decay models, always  $D$ -wave widths are smaller.

In order to disentangle the contribution of the different quark-quark potential pieces, we compare in Table 5 the results of the full model with the ones taken into account only the time-like component of the confinement potential. These last results can be compared with those of Ref. [14] which includes the same pieces of the current although in a slightly different model.

It seems that results including only time-like vector confinement component are better than those of the full model. However, if one looks to the ratios between the different decay channels (Table 6) none of the models are able to reproduce the experimental data. This fact suggest that the dynamics of the charmonium strong decays is far from be a simple process and more Fock components of the wave function can be involved in the decay [30].

## 5. Conclusions

Microscopic models of meson strong decays into two mesons depend on the transition Hamiltonian which drives the decay mechanism. We have developed a model in which the full Hamiltonian that determines the spectrum is used for the decay. In general, the obtained total decay widths are lower than the experimental data although the order of magnitude is reproduced without any free parameter.

It seems that, considering only the confinement time-like components, the agreement with the experimental data is improved. This fact seems to be in line with the conclusions of Ref. [21]. The authors stated that the Dirac structure of confinement should be of a time-like nature which dynamically generates an effective scalar interaction as required by the hadron spectroscopy. However, fine details of the charmonium decays, like the ratios between different decay channels, are not reproduced by any model which suggests that the strong decays into charmed mesons is still an open problem.

## Acknowledgements

This work has been partially funded by Ministerio de Ciencia y Tecnología under Contract No. FPA2010-21750-C02-02, by the European Community-Research Infrastructure Integrating Activity 'Study of Strongly Interacting Matter' (HadronPhysics3 Grant No. 283286), by the Spanish Ingenio-Consolider 2010 Program CPAN (CSD2007-00042) and also, in part, by the U.S. Department of Energy, Office of Nuclear Physics, under contract DE-AC02-06CH11357.

## Appendix A. Matrix elements in the microscopic model

### Appendix A.1. Transition operator

If one considers only the contributions in which a quark-antiquark pair is created, the interaction Hamiltonian in Eq. (9) reduces to the following transition operator

$$\begin{aligned}
T = & \int d^3x d^3y \frac{1}{2} K(|\vec{x} - \vec{y}|) \int \frac{d^3p_1 d^3p_2 d^3p_3 d^3p_4}{(2\pi)^6} \sqrt{\frac{m_1 m_2 m_3 m_4}{E_{\vec{p}_1} E_{\vec{p}_2} E_{\vec{p}_3} E_{\vec{p}_4}}} \sum_{r_1} \sum_{r_2} \sum_{r_3} \sum_{r_4} \\
& [ + b_{r_1}(\vec{p}_1) b_{r_2}^\dagger(\vec{p}_2) a_{r_3}^\dagger(\vec{p}_3) b_{r_4}^\dagger(\vec{p}_4) [\bar{v}_{r_1}(\vec{p}_1) \Gamma v_{r_2}(\vec{p}_2)] [\bar{u}_{r_3}(\vec{p}_3) \Gamma v_{r_4}(\vec{p}_4)] e^{+i(\vec{p}_1 - \vec{p}_2) \cdot \vec{x}} e^{-i(\vec{p}_3 + \vec{p}_4) \cdot \vec{y}} \\
& + a_{r_1}^\dagger(\vec{p}_1) a_{r_2}(\vec{p}_2) a_{r_3}^\dagger(\vec{p}_3) b_{r_4}^\dagger(\vec{p}_4) [\bar{u}_{r_1}(\vec{p}_1) \Gamma u_{r_2}(\vec{p}_2)] [\bar{u}_{r_3}(\vec{p}_3) \Gamma v_{r_4}(\vec{p}_4)] e^{-i(\vec{p}_1 - \vec{p}_2) \cdot \vec{x}} e^{-i(\vec{p}_3 + \vec{p}_4) \cdot \vec{y}} \\
& + a_{r_1}^\dagger(\vec{p}_1) b_{r_2}^\dagger(\vec{p}_2) b_{r_3}(\vec{p}_3) b_{r_4}^\dagger(\vec{p}_4) [\bar{u}_{r_1}(\vec{p}_1) \Gamma v_{r_2}(\vec{p}_2)] [\bar{v}_{r_3}(\vec{p}_3) \Gamma v_{r_4}(\vec{p}_4)] e^{-i(\vec{p}_1 + \vec{p}_2) \cdot \vec{x}} e^{+i(\vec{p}_3 - \vec{p}_4) \cdot \vec{y}} \\
& + a_{r_1}^\dagger(\vec{p}_1) b_{r_2}^\dagger(\vec{p}_2) a_{r_3}^\dagger(\vec{p}_3) a_{r_4}(\vec{p}_4) [\bar{u}_{r_1}(\vec{p}_1) \Gamma v_{r_2}(\vec{p}_2)] [\bar{u}_{r_3}(\vec{p}_3) \Gamma u_{r_4}(\vec{p}_4)] e^{-i(\vec{p}_1 + \vec{p}_2) \cdot \vec{x}} e^{-i(\vec{p}_3 - \vec{p}_4) \cdot \vec{y}} ] ,
\end{aligned} \tag{A.1}$$

where the first term is equal to the third one. This can be seen exchanging the  $\vec{x}$  and  $\vec{y}$  variables in the first term and then, changing  $1 \leftrightarrow 3$  and  $2 \leftrightarrow 4$  particles taking into account the anti-commutation rules of the creation and destruction operators to arrive to the third term. This is possible because the kernel depends on  $\vec{x}$  and  $\vec{y}$  as  $|\vec{x} - \vec{y}|$ . The same occurs with the second and fourth terms. Therefore we have a factor two and we can write the transition operator as

$$\begin{aligned}
T = & \int d^3x d^3y K(|\vec{x} - \vec{y}|) \int \frac{d^3p_1 d^3p_2 d^3p_3 d^3p_4}{(2\pi)^6} \sqrt{\frac{m_1 m_2 m_3 m_4}{E_{\vec{p}_1} E_{\vec{p}_2} E_{\vec{p}_3} E_{\vec{p}_4}}} \sum_{r_1, r_2, r_3, r_4} \\
& [ + a_{r_1}^\dagger(\vec{p}_1) b_{r_2}^\dagger(\vec{p}_2) a_{r_3}^\dagger(\vec{p}_3) a_{r_4}(\vec{p}_4) [\bar{u}_{r_1}(\vec{p}_1) \Gamma v_{r_2}(\vec{p}_2)] [\bar{u}_{r_3}(\vec{p}_3) \Gamma u_{r_4}(\vec{p}_4)] e^{-i(\vec{p}_1 + \vec{p}_2) \cdot \vec{x}} e^{-i(\vec{p}_3 - \vec{p}_4) \cdot \vec{y}} \\
& + a_{r_1}^\dagger(\vec{p}_1) b_{r_2}^\dagger(\vec{p}_2) b_{r_3}(\vec{p}_3) b_{r_4}^\dagger(\vec{p}_4) [\bar{u}_{r_1}(\vec{p}_1) \Gamma v_{r_2}(\vec{p}_2)] [\bar{v}_{r_3}(\vec{p}_3) \Gamma v_{r_4}(\vec{p}_4)] e^{-i(\vec{p}_1 + \vec{p}_2) \cdot \vec{x}} e^{+i(\vec{p}_3 - \vec{p}_4) \cdot \vec{y}} ] ,
\end{aligned} \tag{A.2}$$

where the first and second terms refer to the  $q\bar{q}$  pair creation from the quark line and from the antiquark line, respectively. The diagram representation of these two terms can be seen in Fig. 1, diagrams  $d_{1q}$  and  $d_{1\bar{q}}$ . For illustration we build the result from the diagram  $d_{1q}$ , the transition operator is

$$\begin{aligned}
T = & \int d^3x d^3y K(|\vec{x} - \vec{y}|) \int \frac{d^3p_1 d^3p_2 d^3p_3 d^3p_4}{(2\pi)^6} \sqrt{\frac{m_1 m_2 m_3 m_4}{E_{\vec{p}_1} E_{\vec{p}_2} E_{\vec{p}_3} E_{\vec{p}_4}}} \sum_{r_1, r_2, r_3, r_4} \\
& [ a_{r_1}^\dagger(\vec{p}_1) b_{r_2}^\dagger(\vec{p}_2) a_{r_3}^\dagger(\vec{p}_3) a_{r_4}(\vec{p}_4) [\bar{u}_{r_1}(\vec{p}_1) \Gamma v_{r_2}(\vec{p}_2)] [\bar{u}_{r_3}(\vec{p}_3) \Gamma u_{r_4}(\vec{p}_4)] e^{-i(\vec{p}_1 + \vec{p}_2) \cdot \vec{x}} e^{-i(\vec{p}_3 - \vec{p}_4) \cdot \vec{y}} ] .
\end{aligned} \tag{A.3}$$

The calculation of the diagram  $d_{1\bar{q}}$  can be followed from that of the diagram  $d_{1q}$ . If the initial meson is formed by a quark and an antiquark with equal masses, the contribution of both diagrams to the decay rate is the same and they contribute constructively.

Now, we can integrate in  $\vec{x}$  and  $\vec{y}$

$$T = \int d^3p_1 d^3p_2 d^3p_3 d^3p_4 \tilde{K}(|\vec{Q}|) \delta^{(3)}(\vec{p}_1 + \vec{p}_2 + \vec{p}_3 - \vec{p}_4) \sqrt{\frac{m_1 m_2 m_3 m_4}{E_{\vec{p}_1} E_{\vec{p}_2} E_{\vec{p}_3} E_{\vec{p}_4}}} \sum_{r_1, r_2, r_3, r_4} [a_{r_1}^\dagger(\vec{p}_1) b_{r_2}^\dagger(\vec{p}_2) a_{r_3}^\dagger(\vec{p}_3) a_{r_4}(\vec{p}_4) [\bar{u}_{r_1}(\vec{p}_1) \Gamma v_{r_2}(\vec{p}_2)] [\bar{u}_{r_3}(\vec{p}_3) \Gamma u_{r_4}(\vec{p}_4)]], \quad (\text{A.4})$$

where  $\vec{Q} = \vec{p}_1 + \vec{p}_2 = \vec{p}_4 - \vec{p}_3$  is the momentum transferred,  $\tilde{K}(|\vec{Q}|)$  is the Fourier transform of the kernel  $K(r)$  and the  $\delta$ -function implies the momentum conservation.

#### Appendix A.2. Transition amplitude

We are interested on the transition amplitude for the reaction  $(\alpha\beta)_A \rightarrow (\delta\epsilon)_B + (\lambda\rho)_C$ . In the center-of-mass reference system of meson  $A$  one has  $\vec{K}_A = \vec{K}_0 = 0$  and the matrix element factorizes as follow

$$\langle BC|T|A\rangle = \delta^{(3)}(\vec{K}_0) \mathcal{M}_{A \rightarrow BC}. \quad (\text{A.5})$$

The initial state in second quantization is

$$|A\rangle = \int d^3p_\alpha d^3p_\beta \delta^{(3)}(\vec{K}_A - \vec{P}_A) \phi_A(\vec{p}_A) a_\alpha^\dagger(\vec{p}_\alpha) b_\beta^\dagger(\vec{p}_\beta) |0\rangle, \quad (\text{A.6})$$

where  $\alpha$  ( $\beta$ ) are the spin, flavor and color quantum numbers of the quark (antiquark). The wave function  $\phi_A(\vec{p}_A)$  denotes a meson  $A$  in a color singlet with an isospin  $I_A$  with projection  $M_{I_A}$ , a total angular momentum  $J_A$  with projection  $M_A$ ,  $J_A$  is the coupling of angular momentum  $L_A$  and spin  $S_A$ . The  $\vec{p}_\alpha$  and  $\vec{p}_\beta$  are the momentum of quark and antiquark, respectively. The  $\vec{P}_A$  and  $\vec{p}_A$  are the total and relative momentum of the  $(\alpha\beta)$  quark-antiquark pair within the meson  $A$ . The final state is more complicated than the initial

one because it is a two-meson state. It can be written as

$$\begin{aligned}
|BC\rangle &= \frac{1}{\sqrt{1 + \delta_{BC}}} \int d^3 K_B d^3 K_C \sum_{m, M_{BC}} \langle J_{BC} M_{BC} l m | J_T M_T \rangle \delta^{(3)}(\vec{K} - \vec{K}_0) \delta(k - k_0) \\
&\quad \frac{Y_{lm}(\hat{k})}{k} \sum_{M_B, M_C, M_{I_B}, M_{I_C}} \langle J_B M_B J_C M_C | J_{BC} M_{BC} \rangle \langle I_B M_{I_B} I_C M_{I_C} | I_A M_{I_A} \rangle \\
&\quad \int d^3 p_\delta d^3 p_\epsilon d^3 p_\lambda d^3 p_\rho \delta^{(3)}(\vec{K}_B - \vec{P}_B) \delta^{(3)}(\vec{K}_C - \vec{P}_C) \\
&\quad \phi_B(\vec{p}_B) \phi_C(\vec{p}_C) a_\delta^\dagger(\vec{p}_\delta) b_\epsilon^\dagger(\vec{p}_\epsilon) a_\lambda^\dagger(\vec{p}_\lambda) b_\rho^\dagger(\vec{p}_\rho) |0\rangle,
\end{aligned} \tag{A.7}$$

where we have followed the notation of meson  $A$  for the mesons  $B$  and  $C$ . We assume that the final state of mesons  $B$  and  $C$  is a spherical wave with angular momentum  $l$ . The relative and total momentum of mesons  $B$  and  $C$  are  $\vec{k}_0$  and  $\vec{K}_0$ . The total spin  $J_{BC}$  is obtained coupling the total angular momentum of mesons  $B$  and  $C$ , and  $J_T$  is the coupling of  $J_{BC}$  and  $l$ .

The diagrams that contribute to the reaction and are allowed by the transition operator are shown in Fig. 1. Two of them are coming from the quark line,  $d_{1q}$  and  $d_{2q}$ , and take into account the different rearrangement of the quarks and antiquarks in the final mesons. The other two diagrams are referred to the antiquark line,  $d_{1\bar{q}}$  and  $d_{2\bar{q}}$ . We have different cases:

- Case in which  $\alpha = \mu = \bar{\beta}$ . The two diagrams,  $d_{1q}$  and  $d_{2q}$ , contribute to the decay amplitude. The contribution of diagram  $d_{1q}$  is  $M_{A \rightarrow BC}$  and the contribution from diagram  $d_{2q}$  can be calculated from the amplitude of the  $d_{1q}$  diagram changing meson  $B$  and  $C$  ( $M_{A \rightarrow CB}$ ), so the total amplitude is given by

$$\mathcal{M}_{A \rightarrow BC} = M_{A \rightarrow BC} + (-1)^{I_B + I_C - I_A + J_B + J_C - J_{BC} + l} M_{A \rightarrow CB}. \tag{A.8}$$

- Other case. Only one of the two diagrams contribute to the amplitude

$$\mathcal{M}_{A \rightarrow BC} = M_{A \rightarrow BC}. \tag{A.9}$$

If the quark and antiquark in the original meson are the same, then the contribution of diagram  $d_{1q}$  ( $d_{2q}$ ) is equal to the diagram  $d_{1\bar{q}}$  ( $d_{2\bar{q}}$ ) and both contribute constructively. In other case they have to be calculated separately.

When the initial  $A$  meson has definite  $C$ -parity we have to use final states with definite  $C$ -parity. If  $\mathcal{CB} = C$  the state has definite  $C$ -parity and the amplitude is given by the above rules. If  $\mathcal{CB} \neq C$  then the appropriate  $C$ -parity combination has to be taken and this gives a factor  $\sqrt{2}$  in the amplitude (or the amplitude cancels for the wrong  $C$ -parity).

For illustration we build the result from the diagram  $d_{1q}$  ( $M_{A \rightarrow BC}$ ). The amplitude is a product of a Fermi signature phase, a color factor, a flavor factor and a spin-space overlap integral

$$M_{A \rightarrow BC} = \mathcal{I}_{\text{signature}} \times \mathcal{I}_{\text{color}} \times \mathcal{I}_{\text{flavor}} \times \mathcal{I}_{\text{spin-space}}. \quad (\text{A.10})$$

*Appendix A.2.1. Fermi signature phase*

The Fermi signature can be read off from the diagram as the number of line crossings because it arises from the ordering of the quark and antiquark operators. In the case of  $d_{1q}$  diagram we have

$$I_{\text{signature}} = (-1)^3 = -1. \quad (\text{A.11})$$

*Appendix A.2.2. Color factor*

As all mesons are color singlet  $q\bar{q}$  states the color term is given by

$$\mathcal{I}_{\text{color}} = \frac{1}{3^{\frac{3}{2}}} \sum_a \text{Tr} \left[ \frac{\lambda^a}{2} \frac{\lambda^a}{2} \right] = \frac{4}{3^{\frac{3}{2}}}. \quad (\text{A.12})$$

*Appendix A.2.3. Flavor factor*

For the flavor sector we have

$$\mathcal{I}_{\text{flavor}} = (-1)^{t_\alpha + t_\beta + I_A} \sqrt{(2I_B + 1)(2I_C + 1)} \begin{Bmatrix} t_\beta & I_C & t_\mu \\ I_B & t_\alpha & I_A \end{Bmatrix}, \quad (\text{A.13})$$

where  $t_\xi$  is the isospin of a given quark or antiquark  $\xi$ . Note that the isospin operator in the creation vertex is  $u\bar{u} + d\bar{d} + s\bar{s}$ .

Appendix A.2.4. Spin-space factor

The spin-space overlap integral for the diagram  $d_{1q}$ :  $1 \leftrightarrow \mu$ ,  $2 \leftrightarrow \nu$ ,  $3 \leftrightarrow \delta'$  and  $4 \leftrightarrow \alpha'$ , reads as follow

$$\begin{aligned}
\mathcal{I}_{\text{spin-space}} &= \frac{1}{\sqrt{1 + \delta_{BC}}} \sum_{m, M_{BC}, M_B, M_C} \langle J_{BC} M_{BC} l m | J_T M_T \rangle \langle J_B M_B J_C M_C | J_{BC} M_{BC} \rangle \\
&\int d^3 K_B d^3 K_C d^3 p_\delta d^3 p_\epsilon d^3 p_\lambda d^3 p_\rho d^3 p_\mu d^3 p_\nu d^3 p_{\delta'} d^3 p_{\alpha'} d^3 p_\alpha d^3 p_\beta \sqrt{\frac{m_\mu m_\nu m_{\delta'} m_{\alpha'}}{E_{\vec{p}_\mu} E_{\vec{p}_\nu} E_{\vec{p}_{\delta'}} E_{\vec{p}_{\alpha'}}}} \\
&\delta^{(3)}(\vec{K} - \vec{K}_0) \delta(k - k_0) \delta^{(3)}(\vec{K}_B - \vec{P}_B) \delta^{(3)}(\vec{K}_C - \vec{P}_C) \delta^{(3)}(\vec{P}_A) \frac{Y_{lm}(\hat{k})}{k} \\
&\phi_B(\vec{p}_B) \phi_C(\vec{p}_C) \phi_A(\vec{p}_A) K(|\vec{p}_\mu + \vec{p}_\nu|) \delta^{(3)}(\vec{p}_\mu + \vec{p}_\nu + \vec{p}_{\delta'} - \vec{p}_{\alpha'}) \\
&\sum_{\alpha', \delta', \mu, \nu} \delta_{\alpha' \alpha} \delta^{(3)}(\vec{p}_{\alpha'} - \vec{p}_\alpha) \delta_{\delta' \delta} \delta^{(3)}(\vec{p}_{\delta'} - \vec{p}_\delta) \delta_{\epsilon \nu} \delta^{(3)}(\vec{p}_\epsilon - \vec{p}_\nu) \delta_{\lambda \mu} \delta^{(3)}(\vec{p}_\lambda - \vec{p}_\mu) \\
&\delta_{\rho \beta} \delta^{(3)}(\vec{p}_\rho - \vec{p}_\beta) [\bar{u}_\mu(\vec{p}_\mu) \Gamma v_\nu(\vec{p}_\nu)] [\bar{u}_{\delta'}(\vec{p}_{\delta'}) \Gamma u_{\alpha'}(\vec{p}_{\alpha'})].
\end{aligned} \tag{A.14}$$

Now using some  $\delta$ -functions in momentum and spin of quarks (antiquarks), we can simplify the above expression

$$\begin{aligned}
\mathcal{I}_{\text{spin-space}} &= \frac{1}{\sqrt{1 + \delta_{BC}}} \sum_{m, M_{BC}, M_B, M_C} \langle J_{BC} M_{BC} l m | J_T M_T \rangle \langle J_B M_B J_C M_C | J_{BC} M_{BC} \rangle \\
&\int d^3 K_B d^3 K_C d^3 p_\delta d^3 p_\rho d^3 p_\mu d^3 p_\nu d^3 p_\alpha d^3 p_\beta \sqrt{\frac{m_\mu m_\nu m_\delta m_\alpha}{E_{\vec{p}_\mu} E_{\vec{p}_\nu} E_{\vec{p}_\delta} E_{\vec{p}_\alpha}}} \\
&\delta^{(3)}(\vec{K} - \vec{K}_0) \delta(k - k_0) \delta^{(3)}(\vec{K}_B - \vec{P}_B) \delta^{(3)}(\vec{K}_C - \vec{P}_C) \delta^{(3)}(\vec{P}_A) \frac{Y_{lm}(\hat{k})}{k} \\
&\phi_B(\vec{p}_B) \phi_C(\vec{p}_C) \phi_A(\vec{p}_A) K(|\vec{p}_\mu + \vec{p}_\nu|) \delta^{(3)}(\vec{p}_\delta - (\vec{p}_\alpha - \vec{p}_\mu - \vec{p}_\nu)) \\
&\delta_{\rho \beta} \delta^{(3)}(\vec{p}_\rho - \vec{p}_\beta) [\bar{u}_\mu(\vec{p}_\mu) \Gamma v_\nu(\vec{p}_\nu)] [\bar{u}_\delta(\vec{p}_\delta) \Gamma u_\alpha(\vec{p}_\alpha)].
\end{aligned} \tag{A.15}$$

The nonrelativistic reduction of Eq. (A.15) without specifying the  $JKJ$  decay model is

$$\begin{aligned}
\mathcal{I}_{\text{spin-space}} &= \frac{1}{\sqrt{1 + \delta_{BC}}} \sum_{m, M_{BC}, M_B, M_C} \langle J_{BC} M_{BC} l m | J_T M_T \rangle \langle J_B M_B J_C M_C | J_{BC} M_{BC} \rangle \\
&\int d^3 K_B d^3 K_C d^3 p_\delta d^3 p_\rho d^3 p_\mu d^3 p_\nu d^3 p_\alpha d^3 p_\beta \delta^{(3)}(\vec{K} - \vec{K}_0) \delta(k - k_0) \frac{Y_{lm}(\hat{k})}{k} \\
&\delta^{(3)}(\vec{K}_B - \vec{P}_B) \delta^{(3)}(\vec{K}_C - \vec{P}_C) \delta^{(3)}(\vec{P}_A) \phi_B(\vec{p}_B) \phi_C(\vec{p}_C) \phi_A(\vec{p}_A) \\
&K(|\vec{p}_\mu + \vec{p}_\nu|) \delta^{(3)}(\vec{p}_\delta - (\vec{p}_\alpha - \vec{p}_\mu - \vec{p}_\nu)) \delta_{\rho\beta} \delta^{(3)}(\vec{p}_\rho - \vec{p}_\beta) \\
&\lim_{v/c \rightarrow 0} [\bar{u}_\mu(\vec{p}_\mu) \Gamma v_\nu(\vec{p}_\nu)] \lim_{v/c \rightarrow 0} [\bar{u}_\delta(\vec{p}_\delta) \Gamma u_\alpha(\vec{p}_\alpha)].
\end{aligned} \tag{A.16}$$

We require spin matrix elements which involve the nonrelativistic  $\mathcal{O}(p/m)$  matrix elements of Dirac bilinears with  $\Gamma = I, \gamma^0, \vec{\gamma}$  and Pauli spin matrix elements. These are

$$\begin{aligned}
\lim_{v/c \rightarrow 0} [\bar{u}_\mu(\vec{p}_\mu) I v_\nu(\vec{p}_\nu)] &= \frac{1}{2m_\mu} (\vec{p}_\nu - \vec{p}_\mu) \cdot \langle \mu | \vec{\sigma} | \nu \rangle \\
&= -\frac{1}{2m_\mu} \sqrt{2^5 \pi} \left[ \mathcal{Y}_1 \left( \frac{\vec{p}_\mu - \vec{p}_\nu}{2} \right) \otimes \left( \frac{1 \ 1}{2 \ 2} \right) 1 \right]_0, \\
\lim_{v/c \rightarrow 0} [\bar{u}_\mu(\vec{p}_\mu) \gamma^0 v_\nu(\vec{p}_\nu)] &= \frac{1}{2m_\mu} (\vec{p}_\nu + \vec{p}_\mu) \cdot \langle \mu | \vec{\sigma} | \nu \rangle \\
&= +\frac{1}{2m_\mu} \sqrt{2^3 \pi} \left[ \mathcal{Y}_1(\vec{p}_\nu + \vec{p}_\mu) \otimes \left( \frac{1 \ 1}{2 \ 2} \right) 1 \right]_0, \\
\lim_{v/c \rightarrow 0} [\bar{u}_\mu(\vec{p}_\mu) \vec{\gamma} v_\nu(\vec{p}_\nu)] &= \langle \mu | \vec{\sigma} | \nu \rangle,
\end{aligned} \tag{A.17}$$

and

$$\begin{aligned}
\lim_{v/c \rightarrow 0} [\bar{u}_\mu(\vec{p}_\mu) I u_\nu(\vec{p}_\nu)] &= \delta_{\mu\nu}, \\
\lim_{v/c \rightarrow 0} [\bar{u}_\mu(\vec{p}_\mu) \gamma^0 u_\nu(\vec{p}_\nu)] &= \delta_{\mu\nu}, \\
\lim_{v/c \rightarrow 0} [\bar{u}_\mu(\vec{p}_\mu) \vec{\gamma} u_\nu(\vec{p}_\nu)] &= \frac{1}{2m_\nu} [(\vec{p}_\nu + \vec{p}_\mu) \delta_{\mu\nu} - i \langle \mu | \vec{\sigma} | \nu \rangle \times (\vec{p}_\mu - \vec{p}_\nu)],
\end{aligned} \tag{A.18}$$

where we have used the relation

$$\vec{Y}_1 \cdot \langle \vec{\sigma} \rangle = -\sqrt{3} [Y_1 \otimes \langle \vec{\sigma} \rangle]_0 = \sqrt{6} \left[ Y_1 \otimes \left( \frac{1 \ 1}{2 \ 2} \right) 1 \right]_0. \tag{A.19}$$



Then, the expression for the different contributions are

- $sKs$  interaction

$$\begin{aligned}
\mathcal{I}_{\text{spin-space}}^{sKs} &= \frac{-1}{\sqrt{1 + \delta_{BC}}} \frac{1}{2m_\nu} \sqrt{2^5 \pi} \int d^3 K_B d^3 K_C d^3 p_\alpha d^3 p_\beta d^3 p_\mu d^3 p_\nu d^3 p_\delta \\
&\delta^{(3)}(\vec{K} - \vec{K}_0) \delta^{(3)}(\vec{K}_B - \vec{P}_B) \delta^{(3)}(\vec{K}_C - \vec{P}_C) \delta^{(3)}(\vec{P}_A) \frac{\delta(k - k_0)}{k} \\
&\delta^{(3)}(\vec{p}_\delta - (\vec{p}_\alpha - \vec{p}_\mu - \vec{p}_\nu)) K(|\vec{p}_\mu + \vec{p}_\nu|) \\
&\langle \left[ [\phi_B(\vec{p}_B)(s_\alpha s_\nu) S_B] J_B [\phi_C(\vec{p}_C)(s_\mu s_\beta) S_C] J_C \right] J_{BC} Y_l(\hat{k}) \Big] J_T | \\
&| \left[ [\phi_A(\vec{p}_A)(s_\alpha s_\beta) S_A] J_A \left[ \mathcal{Y}_1 \left( \frac{\vec{p}_\mu - \vec{p}_\nu}{2} \right) (s_\mu s_\nu) 1 \right] 0 \right] J_A \rangle.
\end{aligned} \tag{A.20}$$

- $j^0 K j^0$  interactions

$$\begin{aligned}
\mathcal{I}_{\text{spin-space}}^{j^0 K j^0} &= \frac{1}{\sqrt{1 + \delta_{BC}}} \frac{1}{2m_\nu} \sqrt{2^3 \pi} \int d^3 K_B d^3 K_C d^3 p_\alpha d^3 p_\beta d^3 p_\mu d^3 p_\nu d^3 p_\delta \\
&\delta^{(3)}(\vec{K} - \vec{K}_0) \delta^{(3)}(\vec{K}_B - \vec{P}_B) \delta^{(3)}(\vec{K}_C - \vec{P}_C) \delta^{(3)}(\vec{P}_A) \frac{\delta(k - k_0)}{k} \\
&\delta^{(3)}(\vec{p}_\delta - (\vec{p}_\alpha - \vec{p}_\mu - \vec{p}_\nu)) K(|\vec{p}_\mu + \vec{p}_\nu|) \\
&\langle \left[ [\phi_B(\vec{p}_B)(s_\alpha s_\nu) S_B] J_B [\phi_C(\vec{p}_C)(s_\mu s_\beta) S_C] J_C \right] J_{BC} Y_l(\hat{k}) \Big] J_T | \\
&| \left[ [\phi_A(\vec{p}_A)(s_\alpha s_\beta) S_A] J_A \left[ \mathcal{Y}_1(\vec{p}_\mu + \vec{p}_\nu)(s_\mu s_\nu) 1 \right] 0 \right] J_A \rangle.
\end{aligned} \tag{A.21}$$

- $j^T K j^T$  interactions

$$\begin{aligned}
\mathcal{I}_{\text{spin-space}}^{j^T K j^T} &= \frac{1}{\sqrt{1 + \delta_{BC}}} \sum_{m, M_{BC}, M_B, M_C} \langle J_{BC} M_{BC} l m | J_T M_T \rangle \langle J_B M_B J_C M_C | J_{BC} M_{BC} \rangle \\
&\int d^3 K_B d^3 K_C d^3 p_\delta d^3 p_\rho d^3 p_\mu d^3 p_\nu d^3 p_\alpha d^3 p_\beta \delta^{(3)}(\vec{K} - \vec{K}_0) \delta(k - k_0) \frac{Y_{lm}(\hat{k})}{k} \\
&\delta^{(3)}(\vec{K}_B - \vec{P}_B) \delta^{(3)}(\vec{K}_C - \vec{P}_C) \delta^{(3)}(\vec{P}_A) \phi_B(\vec{p}_B) \phi_C(\vec{p}_C) \phi_A(\vec{p}_A) \\
&K(|\vec{p}_\mu + \vec{p}_\nu|) \delta^{(3)}(\vec{p}_\delta - (\vec{p}_\alpha - \vec{p}_\mu - \vec{p}_\nu)) \delta_{\rho\beta} \delta^{(3)}(\vec{p}_\rho - \vec{p}_\beta) \\
&\lim_{v/c \rightarrow 0} [\bar{u}_\mu(\vec{p}_\mu) \gamma^i v_\nu(\vec{p}_\nu)] \left( \delta_{ij} - \frac{Q_i Q_j}{\vec{Q}^2} \right) \lim_{v/c \rightarrow 0} [\bar{u}_\delta(\vec{p}_\delta) \gamma^j u_\alpha(\vec{p}_\alpha)].
\end{aligned} \tag{A.22}$$

The procedure followed to solve the above spin-space overlap integrals is similar to that of Ref. [28].

## References

- [1] J. J. Aubert, et al., Phys. Rev. Lett. 33 (1974) 1404–1406.
- [2] J. E. Augustin, et al., Phys. Rev. Lett. 33 (1974) 1406–1408.
- [3] T. Appelquist, H. D. Politzer, Phys. Rev. Lett. 34 (1975) 43–45.
- [4] E. Eichten, K. Gottfried, T. Kinoshita, J. Kogut, K. D. Lane, T. M. Yan, Phys. Rev. Lett. 34 (1975) 369–372.
- [5] L. Micu, Nucl. Phys. B10 (1969) 521–526.
- [6] A. Le Yaouanc, L. Oliver, O. Pène, J. C. Raynal, Phys. Rev. D 8 (1973) 2223–2234.
- [7] A. Le Yaouanc, L. Oliver, O. Pène, J.-C. Raynal, Phys. Rev. D 9 (1974) 1415–1419.
- [8] Since the literature is extensive we cite only recent summaries of the  ${}^3P_0$  and related decay models, see H.G. Blundell and S. Godfrey, Phys. Rev. D 53 (1996) 3700 (1996); P.R. Page, Ph.D. thesis, University of Oxford, 1995.
- [9] P. Geiger, E. S. Swanson, Phys. Rev. D 50 (1994) 6855–6862.
- [10] R. Kokoski, N. Isgur, Phys. Rev. D 35 (1987) 907–933.
- [11] S. Godfrey, N. Isgur, Phys. Rev. D 32 (1985) 189–231.
- [12] S. Kumano, V. R. Pandharipande, Phys. Rev. D 38 (1988) 146–151.
- [13] E. Eichten, K. Gottfried, T. Kinoshita, K. D. Lane, T. M. Yan, Phys. Rev. D 17 (1978) 3090–3117, 21 (1980) 203.
- [14] E. J. Eichten, K. Lane, C. Quigg, Phys. Rev. D 73 (2006) 014014.
- [15] E. S. Ackleh, T. Barnes, E. S. Swanson, Phys. Rev. D 54 (1996) 6811–6829.

- [16] B.-F. Li, W.-Z. Deng, X.-L. Chen, arXiv:hep-ph/1105.1620.
- [17] S. Dobbs, et al., Phys. Rev. Lett. 101 (2008) 182003.
- [18] J. Lees, et al., arXiv:hep-ex/1102.4565.
- [19] I. Adachi, et al., arXiv:hep-ex/1103.3419.
- [20] J. Vijande, F. Fernández, A. Valcarce, Journal of Physics G: Nuclear and Particle Physics 31 (2005) 481.
- [21] A. P. Szczepaniak, E. S. Swanson, Phys. Rev. D 55 (1997) 1578–1591.
- [22] J. Segovia, A. M. Yasser, D. R. Entem, F. Fernández, Phys. Rev. D 78 (2008) 114033.
- [23] J. Segovia, A. M. Yasser, D. R. Entem, F. Fernández, Phys. Rev. D 80 (2009) 054017.
- [24] E. Hiyama, Y. Kino, M. Kamimura, Prog. Part. Nucl. Phys. 51 (2003) 223–307.
- [25] J. Beringer, et al., Phys. Rev. D 86 (2012) 010001.
- [26] X. L. Wang, et al., Phys. Rev. Lett. 99 (2007) 142002.
- [27] G. Pakhlova, et al., Phys. Rev. Lett. 101 (2008) 172001.
- [28] R. Bonnaz, B. Silvestre-Brac, Few-Body Systems 27 (3) (1999) 163–187.
- [29] J. Segovia, D. Entem, F. Fernández, Physics Letters B 715 (45) (2012) 322 – 327.
- [30] D. Entem, P. Ortega, F. Fernandez, in: The XIV International Conference on Hadron Spectroscopy, 2011, eConf C110613 (2011); arXiv:hep-ph/1109.0311.

Meson	State	Channel	$\Gamma_{3P_0}$	$\mathcal{B}_{3P_0}$	$\Gamma_{\text{Mic.}}$	$\mathcal{B}_{\text{Mic.}}$
$\psi(3770)$	$1^3D_1$	$D^+D^-$	11.34	42.8	8.03	42.3
		$D^0\bar{D}^0$	15.13	57.2	10.94	57.7
		$DD$	26.47	100	18.97	100
		total	26.47		18.97	
$27.5 \pm 0.9$						
$\psi(4040)$	$3^3S_1$	$DD$	4.61	4.1	10.17	26.0
		$DD^*$	22.23	20.0	18.75	47.9
		$D^*D^*$	82.35	74.0	9.06	23.2
		$D_sD_s$	2.08	1.9	1.14	2.9
$80 \pm 10$		total	111.27		39.12	
$\psi(4160)$	$2^3D_1$	$DD$	22.82	19.7	17.03	52.1
		$DD^*$	2.22	1.9	7.38	22.6
		$D^*D^*$	83.73	72.2	5.28	16.2
		$D_sD_s$	0.24	0.2	2.61	7.9
		$D_sD_s^*$	6.94	6.0	0.40	1.2
$103 \pm 8$		total	115.95		32.70	
$X(4360)$	$4^3S_1$	$DD$	8.02	7.0	5.73	5.6
		$DD^*$	8.19	7.2	29.81	29.2
		$D^*D^*$	8.87	7.8	46.46	45.5
		$DD_1$	54.51	47.8	2.18	2.1
		$DD'_1$	4.29	3.8	12.02	11.7
		$DD_2^*$	27.17	23.8	0.56	0.6
		$D_sD_s$	0.07	0.1	1.86	1.8
		$D_sD_s^*$	1.90	1.7	3.36	3.3
		$D_s^*D_s^*$	0.91	0.8	0.17	0.2
$74 \pm 15 \pm 10$		total	113.92		102.15	
$\psi(4415)$	$3^3D_1$	$DD$	15.11	9.5	7.93	18.5
		$DD^*$	5.82	3.7	6.66	15.6
		$D^*D^*$	32.56	20.5	7.23	16.9
		$DD_1$	64.77	40.7	6.06	14.2
		$DD'_1$	6.92	4.4	2.12	5.0
		$DD_2^*$	23.60	14.8	1.82	4.3
		$D^*D_0^*$	7.12	4.5	2.39	5.6
		$D_sD_s$	0.31	0.2	2.22	5.2
		$D_sD_s^*$	0.68	0.4	1.09	2.5
$62 \pm 20$		$D_s^*D_s^*$	2.13	1.3	5.20	12.2
		total	159.01		42.72	

Table 3: Open-flavor strong decay widths, in MeV, and branchings, in %, of  $\psi$  states.

Meson	State	Channel	$\Gamma_{3P_0}$	$\mathcal{B}_{3P_0}$	$\Gamma_{\text{Mic.}}$	$\mathcal{B}_{\text{Mic.}}$
$X(4630)$	$5^3S_1$	$DD$	6.62	3.2	1.44	0.8
		$DD^*$	26.23	12.7	15.82	8.4
		$D^*D^*$	15.57	7.5	30.40	16.2
		$DD_1$	2.88	1.4	18.70	9.9
		$DD'_1$	4.52	2.2	2.58	1.4
		$DD_2^*$	0.00	0.0	21.14	11.2
		$D^*D_0^*$	6.97	3.4	10.10	5.4
		$D^*D_1$	39.21	19.0	22.47	11.9
		$D^*D'_1$	14.35	7.0	26.24	13.9
		$D^*D_2^*$	80.47	39.0	18.28	9.7
		$D_sD_s$	0.92	0.4	1.28	0.7
		$D_sD_s^*$	0.30	0.1	6.70	3.6
		$D_s^*D_s^*$	1.14	0.6	6.34	3.4
		$D_sD_{s1}$	2.82	1.4	0.92	0.5
		$D_sD'_{s1}$	0.79	0.4	0.03	0.0
		$D_sD_{s2}^*$	0.19	0.1	0.22	0.1
		$D_s^*D_{s0}^*$	2.76	1.3	1.30	0.7
		$D_s^*D_{s1}$	0.14	0.1	3.74	2.0
		$D_s^*D'_{s1}$	0.26	0.1	0.29	0.1
		$D_{s0}^*D_{s0}^*$	0.22	0.1	0.23	0.1
$92_{-24-21}^{+40+10}$		total	206.37		188.22	
$X(4660)$	$4^3D_1$	$DD$	10.92	8.1	3.21	2.3
		$DD^*$	7.55	5.6	4.10	2.9
		$D^*D^*$	38.04	28.2	2.67	1.9
		$DD_1$	2.41	1.8	20.51	14.4
		$DD'_1$	0.51	0.4	2.62	1.8
		$DD_2^*$	0.00	0.0	6.75	4.8
		$D^*D_0^*$	3.44	2.5	0.71	0.5
		$D^*D_1$	34.83	25.8	10.89	7.7
		$D^*D'_1$	6.98	5.1	2.96	2.1
		$D^*D_2^*$	21.92	16.2	77.52	54.5
		$D_sD_s$	0.96	0.7	1.46	1.0
		$D_sD_s^*$	0.00	0.0	1.35	0.9
		$D_s^*D_s^*$	0.33	0.2	4.28	3.0
		$D_sD_{s1}$	3.63	2.7	0.0	0.0
		$D_sD'_{s1}$	1.09	0.8	0.62	0.4
		$D_sD_{s2}^*$	0.08	0.1	0.07	0.1
		$D_s^*D_{s0}^*$	1.18	0.9	0.43	0.3
		$D_s^*D_{s1}$	0.48	0.4	0.93	0.6
		$D_s^*D'_{s1}$	0.17	0.1	0.37	0.3
		$D_{s0}^*D_{s0}^*$	0.53	0.4	0.74	0.5
$48 \pm 15 \pm 3$		total	135.06		142.19	

Table 4: Open-flavor strong decay widths, in MeV, and branchings, in %, of  $\psi$  states (Continuation).

Decay	Ref. [14]	$j^0 K j^0$	Mic.	Exp. [25]
$\psi(3770) \rightarrow DD$	20.1	29.8	19.0	$25.6 \pm 3.4$
total	20.1	29.8	19.0	$27.5 \pm 0.9$
$\psi(4040) \rightarrow DD$	0.1	1.4	10.2	
$\psi(4040) \rightarrow DD^*$	33.0	25.2	18.7	
$\psi(4040) \rightarrow D^* D^*$	33.0	35.0	9.1	
$\psi(4040) \rightarrow D_s D_s$	8.0	0.3	1.1	
total	74.0	61.9	39.1	$80 \pm 10$
$\psi(4160) \rightarrow DD$	3.2	25.0	17.0	
$\psi(4160) \rightarrow DD^*$	6.9	0.5	7.4	
$\psi(4160) \rightarrow D^* D^*$	41.9	21.3	5.3	
$\psi(4160) \rightarrow D_s D_s$	5.6	0.03	2.6	
$\psi(4160) \rightarrow D_s D_s^*$	11.0	0.6	0.4	
total	69.2	47.4	32.7	$103 \pm 8$

Table 5: Open-flavor strong decay widths, in MeV, of  $\psi$  states reported in Ref. [14] and our decay rates taking into account the static vector contribution or the full model.

State	Ratio	$j^0 K j^0$	Mic.	${}^3P_0$	Ref. [14]	Measured [25]
$\psi(4040)$	$DD/DD^*$	0.06	0.54	0.21	0.003	$0.24 \pm 0.05 \pm 0.12$
	$D^* D^*/DD^*$	1.39	0.48	3.70	1.0	$0.18 \pm 0.14 \pm 0.03$
$\psi(4160)$	$DD/D^* D^*$	1.17	3.23	0.27	0.076	$0.02 \pm 0.03 \pm 0.02$
	$DD^*/D^* D^*$	0.02	1.40	0.03	0.16	$0.34 \pm 0.14 \pm 0.05$
$\psi(4415)$	$DD/D^* D^*$	1.54	1.10	0.46	-	$0.14 \pm 0.12 \pm 0.03$
	$DD^*/D^* D^*$	0.28	0.92	0.18	-	$0.17 \pm 0.25 \pm 0.03$

Table 6: Open-flavor strong ratios of  $\psi$  states predicted by different decay models and their comparison with the experimental data.